Simulations of spin filtering effects in a quantum point contact

2008 J. Phys.: Condens. Matter 20 164201

(http://iopscience.iop.org/0953-8984/20/16/164201)

J. Phys.: Condens. Matter **20** (2008) 164201 (8pp) doi:10.1088/0953-8984/20/16/164201

Simulations of spin filtering effects in a quantum point contact

R Akis and D K Ferry

Nanostructures Research Group, Department of Electrical Engineering, Arizona State University, Tempe, AZ 85287-5706, USA

Received 15 October 2007, in final form 13 December 2007
Published 1 April 2008
Online at stacks.iop.org/JPhysCM/20/164201

Abstract

In this paper, we review the results of transport simulations that we have done in recent years, of quantum point contacts (QPCs) which incorporate spin-density-functional theory. Besides the usual plateaus at integer multiples of $G_0 = (2e^2/h)$ our calculations yield the type of $\sim 0.7G_0$ features that have now become familiar in experiment, as well as anomalies at other non-integer values. These features appear to be correlated with the formation of an energy barrier structure within the QPC that can be very *strongly* spin dependent. In particular, these can be strong enough that there are circumstances where two spin-down modes may pass through the QPC before any current from the other spin orientation is allowed through. The barriers can be tuned to produce different spin filtering effects and can lead to the formation of a local magnetic moment in the QPC region, which however is only weakly confined in our case. We can also account for the *absence* of plateaus at higher integer values of G_0.

(Some figures in this article are in colour only in the electronic version)

1. Introduction

Quantum point contacts (QPCs) can be formed in semiconductor heterostructures by depositing a pair of metal gates. Biasing the gates creates a quasi-1D channel (i.e. a wire, or a QPC for very short channels) which separates the 2DEG (two-dimensional electron gas) that exists in the heterostructure into source and drain regions and through which current can flow. The conductance for such structures has been found experimentally to be quantized with plateaus at integer multiples of $G_0 = (2e^2/h)$ as a function of gate voltage [1, 2]. These results can be explained within a single electron picture with the conductance being given by the number of modes that can propagate through the QPC [3]. More recent experiments however have found additional non-integer plateaus, in particular a $\sim 0.7G_0$ conductance anomaly that has been observed in QPCs [4–8]. There is some disagreement about the theoretical explanation for this feature [9–13], but the consensus is that electron–electron interactions must be included to account for such effects, which the authors cited above have typically done be incorporating spin-density-functional theory (SDFT) into the transport calculations.

In this paper, we present the results of our own transport calculations using SDFT performed over the last few years, much of which has been presented previously elsewhere [14]. Besides being able to obtain $\sim 0.7G_0$ anomalies similar to experiment, we find that these features can be correlated with the formation of a *spin-dependent* energy barrier structure. With the QPC we studied, we found that these can be particularly strong, and there are instances where *two modes* of spin-down electrons can be almost fully transmitted through the channel before spin-up electrons are allowed through. These barriers rise and fall as a function of the local density and by varying it, the $\sim 0.7G_0$ anomaly can be made to evolve into fully formed plateau at G_0, and additional features can be similarly made more or less prominent. In particular, we can also account for additional experimentally observed features such as anomalies at $\sim 0.25G_0$ [5, 7, 15] and 'missing' plateaus at higher conductances [15, 16]. Our calculations also show the formation of a local magnetic moment in the QPC region as a result of the spin-dependent barrier structure. Recent experiments and supporting theoretical work on coupled QPCs have provided evidence that, not only do such moments exist, they can actually be read out electrically [17–21]. Importantly, we find that these moments are only weakly confined by the spin-dependent barrier structure (it primarily blocks transmission rather than provides confinement) and cannot be associated with a truly bound state.

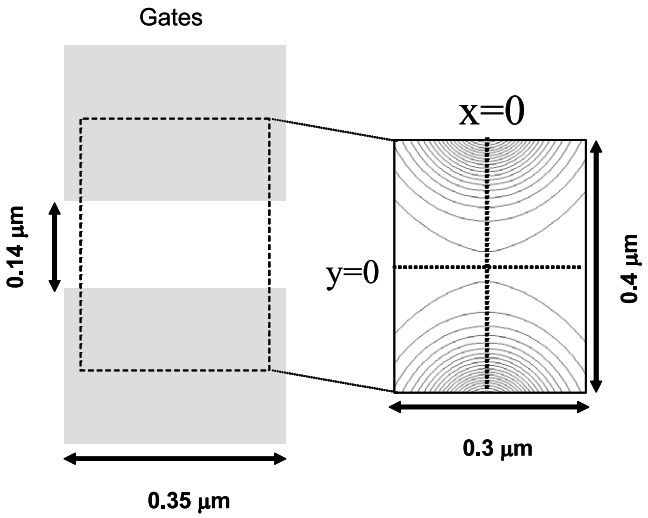

Figure 1. On the left, the split gates that form the model QPC. On the right, the contours of the Timp model confining potential at the level of the 2DEG.

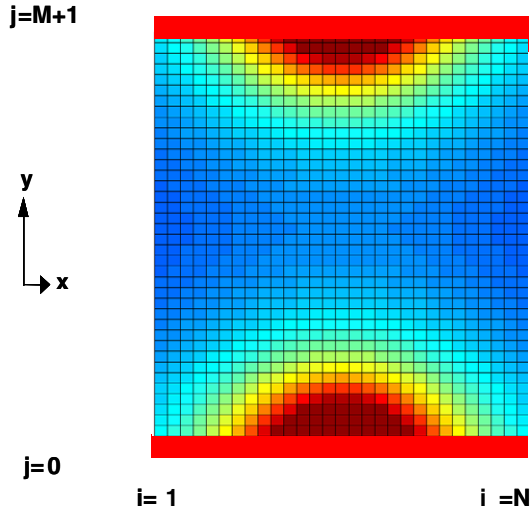

Figure 2. A QPC potential placed inside a waveguide for the purposes of calculation. The grid represents the underlying finite-difference mesh on which the calculations are performed.

2. Theoretical model

We model a QPC formed by split gates as shown in the left panel of figure 1. As a simple starting point, for the initial 2D confining potential generated by these gates, we have used the model potential given by Timp [22]:

$$V_{\rm conf}(x,y) = f\left(\frac{2x-l}{2z_o},\frac{2y+w}{2z_o}\right) - f\left(\frac{2x+l}{2z_o},\frac{2y+w}{2z_o}\right) + f\left(\frac{2x-l}{2z_o},\frac{-2y+w}{2z_o}\right) - f\left(\frac{2x+l}{2z_o},\frac{-2y+w}{2z_o}\right) \tag{1}$$

where

$$f(u,v) = \frac{eV_{\rm g}}{2\pi}\left[\frac{\pi}{2} - \tan^{-1}(u) - \tan^{-1}(v) + \tan^{-1}\left(\frac{uv}{\sqrt{1+u^2+v^2}}\right)\right]. \tag{2}$$

Here l and w are the lithographic width (350 nm) and gap (140 nm) between the electrodes, respectively, and $V_{\rm g}$ is the applied gate voltage, and the vertical distance between the 2DEG and the gate, z_o, has been taken to be 70 nm. The right panel shows the contours of potential that arise for a $V_{\rm g} = -0.55$ V in a domain at the very center of the QPC. It is over this domain, which is actually smaller than the assumed lithographic dimensions of the QPC, that the simulations are performed. We have found it is unnecessary to go further out from the center as the conductance we obtain varies little after more than about five propagating modes are allowed at the outer boundaries of the simulation region.

The potential experienced by the electrons in the QPC is modified when self-consistent effects are explicitly taken into account within that region. Using an advanced Kohn–Sham local spin-density functional theory [23] to account for these interactions, the total potential for spin σ becomes:

$$V^{\sigma}_{\rm tot}(x,y) = V_{\rm conf} + V_{\rm H} + V^{\sigma}_{\rm exch} + V^{\sigma}_{\rm cor}. \tag{3}$$

where $V_{\rm H}$ is the Hartree potential, $V^{\sigma}_{\rm cor}$ is the correlation potential. For these, we have used the expression derived by Tanatar and Ceperly [24]. The exchange potential $V^{\sigma}_{\rm exch}$ we use is that derived by Stern [25]. It should be noted that the local SDFT approximation has its limitations, in particular, it does not yield the proper two-particle correlations that one would obtain from exact diagonalization. However, while an approximation, the densities obtained within the approximation mimics what one would obtain from the exact wavefunction, thus at least partially accounting for the real correlations [26]. Good agreement between SDFT and exact diagonalization results has been obtained in the cases of quantum dots, wires and rings (see [26] for a review) and has been used by other theoretical groups studying the QPC problem, as noted above.

Since there is only strong confinement in one direction, instead of a full two-dimensional treatment of the problem, our approach was to break the QPC into a series of one-dimensional slices perpendicular to the x axis, and solve for the self-consistent potential of each slice *individually* using a method analogous to that originally developed for quantum wires [27, 28]. Figure 2 shows the grid over which we performed such calculations. Following Berggren and Yakimenko [10], a weak Zeeman term ($g\mu_{\rm B}B\sigma \sim 10^{-6}$ eV) is included in the first few iterations of each self-consistent loop to break the initial spin degeneracy. One quantity of particular importance for this calculation is the 1D electron density, $n_{\rm 1D}$. We begin the calculation by setting it at the left boundary of the simulation domain. Working within the usual effective mass, m^*, approximation (this is generally sufficient since we always near the bottom of the conduction band), this density is related to the Fermi energy, $E_{\rm F}$, through

$$n_{\rm 1D} = \sum_{\sigma,m}\left(2m^*(E_{\rm F} - E^{\sigma}_{\rm m})/\hbar\right)^{1/2}/\pi, \tag{4}$$

where $E^{\sigma}_{\rm m}$ are the energies of the modes and the sum is restricted over those that propagate. Since we are considering

a GaAs 2DEG, $m^* = 0.067$. This parameter acts simply as a scaling parameter in our calculation.

Given n_{1D}, one can determine E_F which in turn can be converted to a 2D density. Thus, one can chooses n_{1D} to yield reasonable values that agree with typical measured experimental values of the latter quantity. With regards to this slice by slice method, the E_F at the left boundary is what used to set the n_{1D} values for the individual slices through the device.

In keeping with the results for the self-consistent potential, our conductance calculations are performed on a square finite-difference lattice with lattice constant a. Lattice position can be specified by integers i and j. The conductances for the two spin orientations are computed separately. To lowest order, the 2D Schrödinger equation for electrons of spin σ becomes [29]:

$$-t(\psi^{\sigma}_{i+1,j} + \psi^{\sigma}_{i-1,j} + \psi^{\sigma}_{i,j+1} + \psi^{\sigma}_{i,j-1}) + (V^{\sigma}_{i,j} + 4t)\,\psi^{\sigma}_{i,j} = E^{\sigma}\,\psi^{\sigma}_{i,j}, \qquad \text{where } t = \frac{\hbar^2}{2m^*a^2}, \tag{5}$$

and $V^{\sigma}_{i,j}$ represents the discretized full potential at site i, j and E^{σ} is the energy of the electron with spin σ. For convenience, the QPC is enclosed inside an ideal quantum wire, which extends outward to $\pm\infty$ along the x-axis. This is shown schematically in figure 2. Given a structure $M+1$ lattice points high (with M actual points in the interior being simulated) and N lattice points across, and using the center of the device as the zero reference, then i and j are related to actual position by $x = a(i - (M+1)/2)$ and $y = a(j - N/2)$.

To calculate the transmission through a device, the modes are injected from the left side with unit amplitude. Using (5), one can derive a transfer matrix equation that relates adjacent slices to achieve this purpose. For a structure N slices long, one must thus solve the transfer matrix problem:

$$\begin{bmatrix} \mathbf{t}^{\sigma} \\ \mathbf{0} \end{bmatrix} = \mathbf{T}_0^{-1}\mathbf{T}_N\mathbf{T}_{N-1}\ldots\mathbf{T}_1\,\mathbf{T}_0 \begin{bmatrix} \mathbf{I} \\ \mathbf{r}^{\sigma} \end{bmatrix}, \tag{6}$$

where $\mathbf{t}^{\sigma}$ is a matrix of spin-dependent transmission amplitudes of waves exiting from the right part of the structure, and $\mathbf{r}^{\sigma}$ is the matrix of amplitudes of waves reflected back towards the left. The inclusion of the unit matrix $\mathbf{I}$ ensures that each mode is being sent in with unit amplitude, while $\mathbf{T}_0$ is a matrix consisting of the modes, both propagating and evanescent, calculated by solving the transfer matrix eigenvalue problem in the initial slice of the device. It should be noted that for a good discrete approximation the kind of parabolic dispersion one would expect if the modes were calculated analytically, the lattice constant a should be a small fraction of the Fermi wavelength (~0.1 or smaller). Given $\mathbf{t}^{\sigma}$, one calculate the spin-dependent conductance G^{σ} using the Landauer–Buttiker formula:

$$G^{\sigma} = \frac{2e^2}{h}\sum_{m,n}\frac{v^{\sigma}_n}{v^{\sigma}_m}\left|t^{\sigma}_{m,n}\right|^2, \tag{7}$$

where $t_{n,m}$ represents the transmission amplitude of mode n to mode m, and the summation is only over propagating modes. Here, v^{σ}_n is the velocity of the nth mode, which can be obtained by taking the expectation value of the current operator. Unfortunately, equation (6) in its present form is made numerically unstable by the exponentially growing and decaying contributions of the evanescent modes that accumulate when the product of transfer matrices is taken. Usuki *et al* [29] overcame this difficulty be recasting the transfer matrix problem in terms of an iterative scheme resembling a cascade of scattering matrices [30]. The numerical stability of the Usuki *et al* method stems from the fact that the iterative scheme involves products of some of the original transfer matrices with matrices that are *inverted*. Thus, the exponential factors that cause numerical difficulties when transfer matrices are simply multiplied together end up being canceled out.

Once the transmission coefficients are obtained, the electron wavefunction $\Psi(i, j, k)$ at each site, i, j, and incident mode, k, can be reconstructed using a similar recursive scheme [29, 31]. Given q propagating modes for a given spin σ incident from the left, the 2D probability density at x and y is given by:

$$n^{\mathrm{L}}_{\sigma}(x, y) = n^{\mathrm{L}}_{\sigma}(a(i - (M+1)/2), a(j - N/2)) = \sum_{k=1}^{q}|\psi_{\sigma}(i, j, k)|^2. \tag{8}$$

The superscript, L, is included because this density only takes into account contributions from electron waves incident from the left. In a real situation, waves come from both directions, so that the true 2D density will be the sum over left and right incident wave contributions:

$$n_{\sigma} = n^{\mathrm{L}}_{\sigma} + n^{R}_{\sigma}. \tag{9}$$

Making the assumptions that there is only a vanishingly small potential drop and the device is perfectly symmetric, then these contributions can be taken to be equal, but mirror reversed about the center of the QPC.

Given that the experimental observations generally have all been made at very low temperatures, the calculations shown here have been done zero temperature for the sake of simplicity. Thus, no inelastic scattering events are incorporated into the calculation.

3. Simulation results

In figure 3, we present a surface plot of the *total* conductance (the sum over the two spin channels) versus V_g and n_{1D}. The curves used to construct this surface corresponded to a range of 1.68–2.38 $\times 10^6$ cm^{-1} (E_F = 12.9–14.0 meV, given $V_g = -0.55$ V). For the initial confining potential considered and the density range chosen, we found that there are no actual conductance plateaus at $2G_0$, only points of inflection in the conductance traces in that region, which shift according to the density. We also find that some traces show an actual plateau at ~G_0, while others develop a hump that falls somewhat short of this value, which can even drop below ~$0.5G_0$ as the density is varied. Many individual traces also have pairs of features below ~G_0 and ~$0.5G_0$, respectively. What follows are some representative examples.

In the left-hand panel of figure 4, the conductance is plotted for an illustrative one-dimensional density,

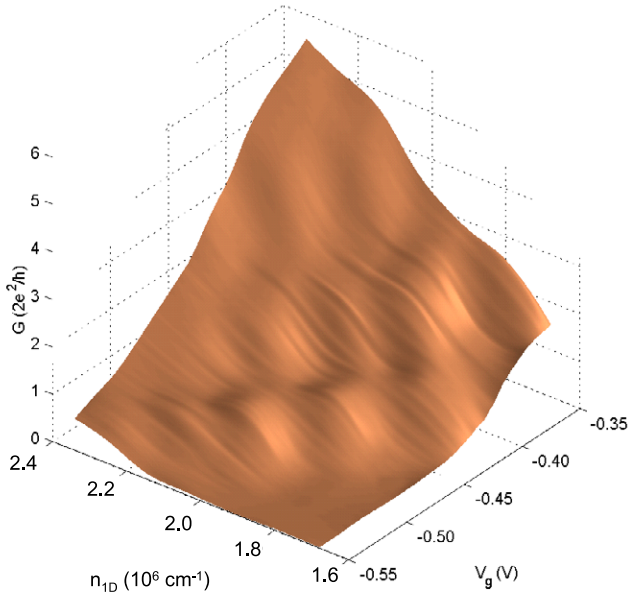

Figure 3. Surface illustrating the total conductance of a QPC, calculated as a function of gate voltage and electron density. For the simulations shown here, we used $M = 69$ and $N = 40$.

$n_{1D} = 2.01 \times 10^6$ cm^{-1} ($E_F = 13.5$ meV). The contributions of the spin-up and spin-down channels to the conductance are also plotted as dashed and dotted lines in the same figure. The total conductance exhibits a sloped region near $\sim 0.8G_0$, rather than a flat plateau at G_0, and there is also a weaker inflection point near $0.3G_0$. Such features are similar to those observed experimentally [4, 5, 7, 15, 16]. From a comparison of the spin-resolved components of the transmission, it is clear that the spin-down contribution dominates the conductance, even up to $\sim G_0$. In fact, the implication in this case is that *two* spin-down modes can be fully transmitted through the QPC, before the first spin-up mode begins to propagate.

Insight into the different transmission characteristics can by obtained by looking at the self-consistent QPC potentials seen by the two spins. Three pairs of potentials are shown as insets in figure 4. In comparison to the bare confining potential, we see that an additional potential barrier structure becomes superimposed upon the QPC when self-consistency is introduced, a structure that depends on whether the spin is up or down, and which weakens as more modes are allowed to pass through the QPC.

Since the spin-dependent barriers in figure 4 show relatively little variation along the y-direction, one can think of them as essentially quasi-one-dimensional. In the right-hand panel of figure 4, we adopt this viewpoint and plot the potentials after averaging them over the y-direction ($\langle V(x, y = y_o)\rangle$, where y_o is the center of the QPC). In case (a), the spin-dependent potentials are equal at the center of the QPC. Away from the center, however, they deviate, with the spin-down potential dropping significantly below that of spin-up, splitting with the latter and developing 'shoulders'. As previously noted in the context of quantum wires [28], this potential splitting, *which can be larger than the level spacing of the modes*, is largely the result of the exchange potential, and will oscillate as a function of the local density. Consequently, the effective barrier height (dependent on the potential and width of the barrier) is lower for spin-down electrons, which are partially transmitted through the QPC while spin-up modes are blocked completely. In case (b) of figure 4, the spin-up

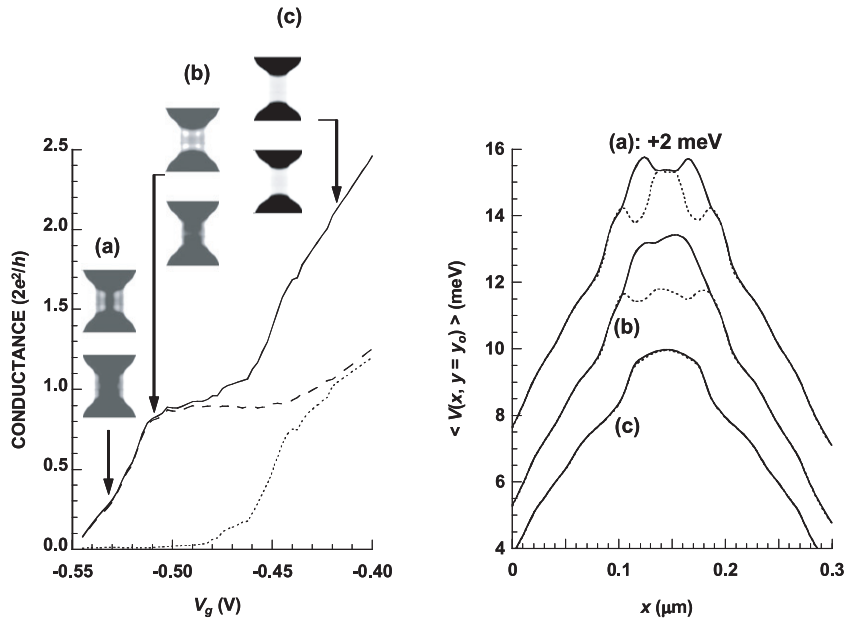

Figure 4. Left: QPC conductance for a one-dimensional density, $n_{1D} = 2.01 \times 10^6$ cm^{-1} ($E_F = 13.5$ meV). The solid line is the total conductance variation, while the dashed and dotted lines show the spin-resolved contributions to the conductance. Also shown are the spin-dependent potential barriers formed in the QPC, at several different gate voltages, with darker shading indicating higher potential. Upper plots show the spin-down barrier, lower ones the spin-up barrier. Right: variation of the average barrier height as a function of position along the direction of current flow, for the three gate voltages indicated by arrows in the left-hand panel. The dotted lines are the barrier for spin-down electrons, the solid line is for spin-up electrons. The potentials for (a) are vertically offset by the indicated energies.

barrier remains high, but the central portion of the spin-down barrier has now collapsed. With this collapse, the first spin-down mode is fully transmitted through the barrier, along with a significant fraction of a second mode, with the same spin, yielding the conductance step near $0.8G_0$. At the same time, transmission of the spin-up modes remains blocked, *so that the QPC functions as a spin filter*. As the gate voltage is gradually made less negative, the QPC gradually opens and the spin-resolved barriers eventually collapse upon one another. This is the situation in case (c) of figure 4, where we see that the two potentials are essentially identical.

We actually find that the effective one-dimensional barriers shown in figure 4 to be quite generic features, and are found in conjunction with every conductance trace used to construct for figure 3. What varies as n_{1D} is changed is the *relative transparency* of these barriers. Whether one sees well formed plateaus, humps or just points of inflection at particular gate voltages depends largely on n_{1D}. Moreover, *one type of feature can be made to evolve into another*. It should be noted that spin-and density-dependent barriers have of course been obtained in numerical studies performed by other authors [10, 11, 32].

While there is convergence of the spin-up and down potentials at the less negative gate voltages, it is evident that the self-consistent potential in case (c) still has the form of an *additional* barrier superimposed upon the initial QPC saddle potential. The presence of this additional barrier prevents the modes from being cleanly transmitted through the QPC, as a result of which the conductance curves in figure 4 show only an *inflection* near $2G_0$, rather than a fully formed plateau. Such behavior has been seen experimentally. A particularly weak plateau at $2G_0$ is displayed in Thomas *et al* for their sample D [4]. Inflections instead of plateaus were observed by Shailos *et al* [15], who used a finger gate to vary the electron density entering the QPC, which we have done here by hand by varying n_{1D} in our simulations. More recently, Gunawan *et al* [16] did experiments on an AlAs QPC which revealed similar behavior as shown here: a well formed $\sim 0.7G_0$ feature accompanied by only inflections at integer values of G_0. However, in that case, the two-dimensional electrons occupied *two* in-plane valleys with elliptical Fermi contours. The lack of well formed plateaus (there expected at multiples of $2G_0$ because of the contribution of the two valleys) was taken as an indication of a broken valley degeneracy in the QPC and that it was acting as a simple 'valley filter' device.

Insight into the formation of plateaus or the lack thereof can be obtained by utilizing an old but still useful model developed by Büttiker [3]. He considered a QPC expressed in terms of saddle potential whose curvature was characterized by two frequencies ω_x and ω_y:

$$V(x, y) = V_0 - \tfrac{1}{2}m^*\omega_x^2 x^2 + \tfrac{1}{2}m^*\omega_y^2 y^2. \tag{10}$$

Here, V_0 is the electrostatic potential at the saddle. Expressed as a sum over modes, n, entering the QPC, the conductance for this model is given by:

$$G = \sum_n \frac{1}{1+\exp(-\pi\,\varepsilon_n)} \qquad \text{where}$$

$$\varepsilon_n = 2\left[E - \hbar\omega_y\left(n+\frac{1}{2}\right) - V_0\right]\Big/\hbar\omega_x. \tag{11}$$

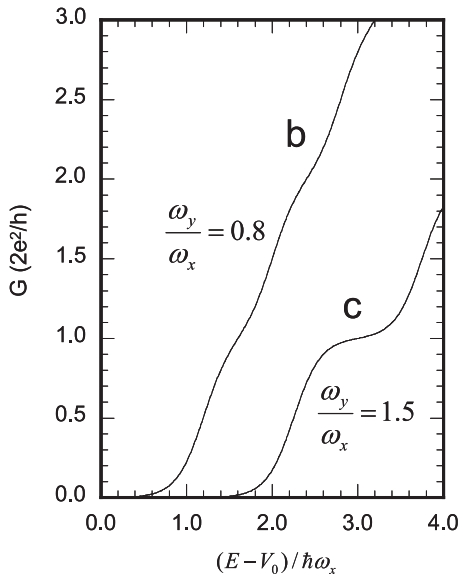

Figure 5. The conductance obtained using Büttiker's formula as a function of normalized energy is plotted for values of ω_y/ω_x obtained by fitting a saddle potential to the self-consistent potentials that were computed at points (b) and (c) in figure 4.

Büttiker found that steps at integer values of G_0 occurred provided that

$$\omega_y/\omega_x \geqslant 1, \tag{12}$$

with the steps becoming progressively flatter the larger this ratio is. What ω_y does is determine the energy separation of the modes at the QPC ($E_n = \hbar\omega_y(n + 1/2)$), while ω_x determines the width of the transition region for the opening of a quantum channel or mode. According to equation (11), if the transition region is small compared to the energy separation, then steps result. We have fitted a saddle potential as described by equation (10) to the fully self-consistent potentials we obtained for the spin-down electrons at points (b), where there is a broad conductance plateau for that spin channel, and (c), where there is an inflection, in figure 4. Those fits yielded a ratio $\omega_y/\omega_x = 0.8$ for (b) and $\omega_y/\omega_x = 1.5$ for (c). Figure 5 shows the results of inputting those fits into equation (11). As one might expect from the preceding discussion, the $\omega_y/\omega_x = 1.5$ curve has a rounded plateau over the energy range displayed, while the $\omega_y/\omega_x = 0.8$ curve yields only inflections instead of real plateaus. Thus, the disappearance of plateaus at less negative gate voltages in figure 4 can be understood in terms of the evolution of the shape of the QPC potential. It should be emphasized that this sort of transition (plateau to inflection point) in individual gate voltage traces only occurs if self-consistency is included in the calculation, at least for the first few modes.

Figure 6 depicts what occurs for a different choice of density. For this plot of the conductance as a function of V_g, we have used $n_{1D} = 1.96 \times 10^6$ cm^{-1} ($E_F = 13.4$ meV). Unlike the previous example, there is now a plateau at G_0. Note as well that steps also occur at $\sim 0.25G_0$ and $\sim 0.5G_0$ in this case. In contrast to figure 4, the 'shoulders' shown by the various potentials are a more prominent here (an example being marked by asterisks in figure 6). The behavior

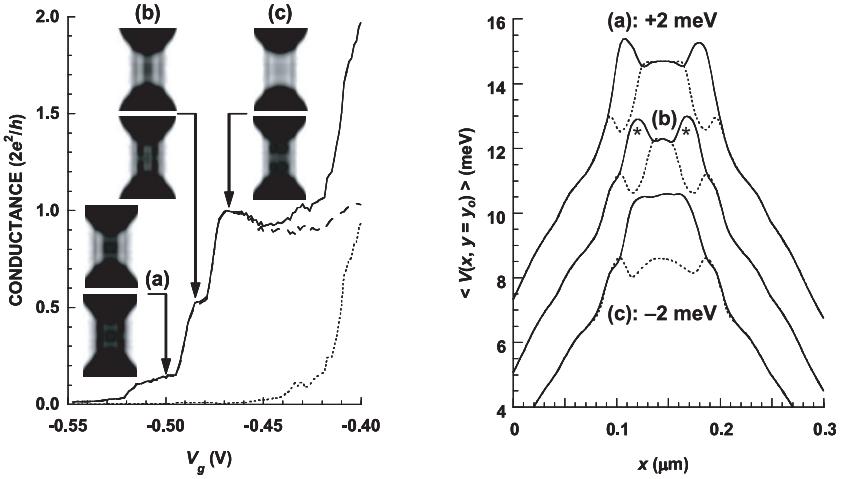

Figure 6. Left: QPC conductance for a one-dimensional density, $n_{1D} = 1.96 \times 10^6$ cm^{-1} ($E_F = 13.4$ meV). The solid line is the total conductance variation, while the dashed and dotted lines show the spin-resolved contributions to the conductance. Also shown are the spin-dependent potential barriers formed in the QPC, at several different gate voltages. Upper plots show the spin-down barrier, lower ones the spin-up barrier. Right: variation of the average barrier height as a function of position along the direction of current flow, for the three gate voltages indicated by arrows in the left-hand panel. The dotted lines are the barrier for spin-down electrons, solid line is for spin-up electrons. The potentials for (a) and (c) are vertically offset by the indicated energies.

shown here is noteworthy since it would appear to show a connection between the presence of quasi-plateaus in the conductance (near $0.25G_0$ and $0.5G_0$), and the formation of a well defined *local potential well* for one spin species. This suggests the possibility that our simulations may reveal a local spin polarization and the formation a local magnetic moment. As mentioned earlier, recent work has provided evidence for the electrical readout of such moments, by studying the characteristics of coupled QPCs [17–21].

In that regard, the ∼0.7 feature has been theoretically associated with the formation of a magnetic moment for quite some time. However, there has been debate over its nature, with two distinct scenarios currently being explored. One of these ascribes the local moment to the spontaneous spin polarization of electrons in the one-dimensional channel [10, 12, 13, 32, 33], while the other may be described as a Kondo-like scenario [9, 11, 34]. In the former scenario, the local moment is viewed as having a ferromagnetic origin, due to the ordering of the electrons spins in the one-dimensional channel when the exchange energy of their Coulomb interaction exceeds their kinetic energy. As such, this magnetic moment is often referred to as *static*. The Kondo approach, on the other hand, is based upon the presence of a dynamic magnetic moment, which originates from the correlated many-body state that is formed between a localized electron in the QPC and the reservoirs connected to it. Although electrons constantly tunnel back and forth between the QPC and the reservoirs, the equivalence of the number of spin-up and spin-down electrons visiting the contact is broken, resulting in a non-zero net spin polarization in the QPC. As such, this scenario is roughly equivalent to the conventional Kondo effect for a spin localized on an impurity, or in a quantum dot [35]. An important issue here is that, while the Kondo model requires the formation of a localized electron state in the QPC [9, 11], other authors [10, 12, 32] have argued that local spin polarization (i.e. moment formation) can arise *without* the formation of such a state. All that is required in the latter case is that a spin-dependent barrier should develop in the QPC, giving rise to different spin-resolved densities.

With above considerations in mind, in figure 7, we investigate the extent to which the spin-dependent barrier structure noted in figure 6, gives rises to a local spin polarization, P, within the QPC region to see to what extent a local magnetic moment is formed. We define this quantity in terms of the total local spin densities, $n_\sigma(x, y)$, as follows:

$$P = \int\int_{\mathrm{QPC}} p(x, y)\,\mathrm{d}x\,\mathrm{d}y, \qquad \text{where}$$

$$p(x, y) = \left[\frac{n_\downarrow(x, y) - n_\uparrow(x, y)}{\int\int_{\mathrm{QPC}} \mathrm{d}u\mathrm{d}v\,\big(n_\downarrow(u, v) + n_\uparrow(u, v)\big)}\right]. \quad (13)$$

Once again, it should be noted that the densities in this calculation represent the sum total for each spin obtained by sending waves into the structure from both the left and the right side of the QPC. Note that since spin-down modes are favorably transmitted in our simulations, we have chosen them as making the positive contribution to the above function. As is evident from the P versus V_g plot, a non-zero polarization is obtained at the lower gate voltages. At higher gate voltages, where the spin-up and down potentials converge, the polarization also vanishes. Interestingly, near the positions of the $0.25G_0$ and $0.5G_0$ features (labeled (a) and (b) respectively), local maximums in P occur, though nothing noteworthy happens in this function when the G_0 plateau is reached at (c).

In the lower panel of figure 7, we examine what is occurring inside the QPC at these three points. In the upper tier of images, the spin-up density for waves incident from the left is plotted for the three cases. As is apparent, the spin-up electron waves never manage to penetrate all the way to the right-hand side of the QPC. The second tier shows what occurs

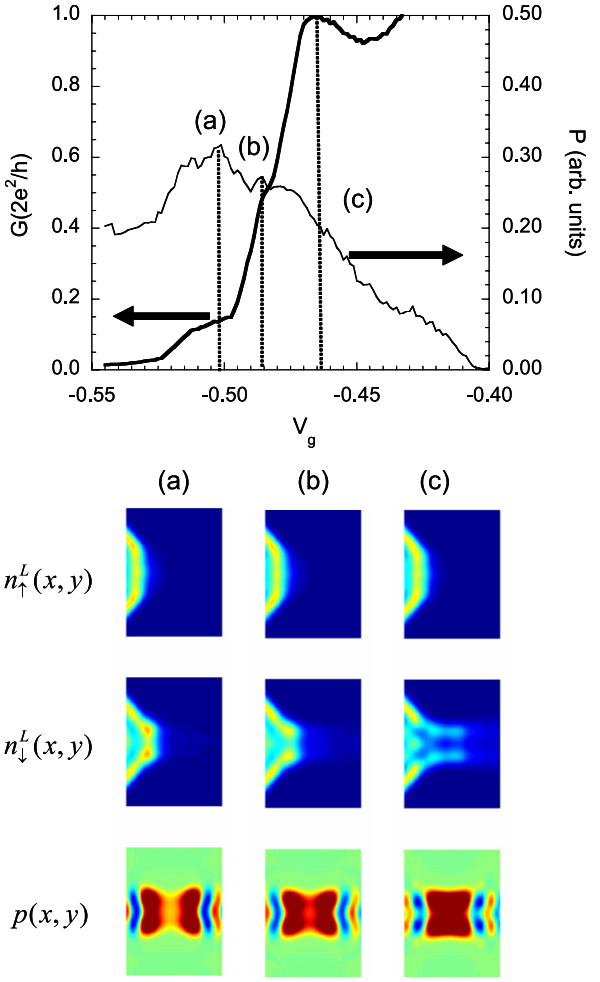

Figure 7. Top panel: the spin polarization (as defined in equation (13)) as a function of gate voltage is plotted for a one-dimensional density, $n_{1D} = 1.96 \times 10^6$ cm^{-1} ($E_F = 13.4$ meV). The conductance from figure 6 is overlaid. Bottom panel: the local densities for spin-up and spin-down (the L indicates waves incident from the left), and the local polarization (which includes contributions from both left and right incident waves) is plotted as a function of x and y in the QPC at the points marked (a), (b), and (c) in the upper panel.

for spin-down. As is evident from the density, two spin-down modes manage to penetrate well into the QPC in each case (note the double peaks). At (a), one can see an exponential tail in the spin-down density on the right-hand side, in keeping with only a single mode being partially transmitted. At (b), now one of the two spin-down modes is being fully transmitted. At (c), both these modes are now fully transmitted. The effects of the 'shoulders' in the potentials, discussed above, are not particularly evident here. The role they play becomes more clear in the lowest tier of images, where we plot $p(x, y)$, the local polarization obtained by considering waves incident from both the left and the right. In each case, this function has a multi-peaked region of high amplitude in the central region of the QPC, meeting up with rippled tails extending to the right and left. Where those tails begin is precisely where the 'shoulders' are in the potentials. At (a) and (b), $p(x, y)$ has four peaks in the central region. At (c), there has been a merging effect, and four have become two. This is a result of the fact that there two spin-down modes can penetrate entirely through the QPC at that point.

While our results show that a local magnetic moment does form at the center of the QPC in the regime where the conductance is less than G_0, it should be emphasized here that in the present case one can not associate it with a strongly localized spin state. The feature we have obtained can be best described as weakly bound. That said, we again note the differences between the results in figure 4, where the comparatively weak 'shouldered' potentials and less well defined local potential wells yielded an inflection point and a hump in the conductance, and the plateaus evident here where such potential features showed up more prominently.

In their numerical study, Starikov *et al* [32] performed calculations for a similar structure to that considered here and found evidence for spin-dependent-barrier formation, reminiscent of that shown in figure 5, but no evidence for the presence of quasi-bound states. In contrast, Hirose *et al* [11] have argued that such localized states are responsible for the Kondo-like characteristics observed in some QPC experiments [7]. The recent work of Yoon *et al* [21], which coupled experiment with theory, indicated robust spin confinement in the system they studied. The suggestion of the preceding results, which represent an intermediate position, is that *both* scenarios may actually be realistic, but dependent upon the specific conditions (i.e. electron density and confining potential) in the QPC channel. With regards to the latter, there are suggestions that there is a significant dependence on the length of the QPC [6, 12], with the amount of spin polarization increasing as the QPC is made longer. We have seen such indications in our calculations. Indeed, some of the simulations we have performed yielded true conductance resonances (instead of just steps or inflection points) when relatively long QPCs were studied. We intend to present this work elsewhere.

4. Conclusions

In conclusion, as in recent experiments on QPCs, our SDFT calculations yield additional structure besides the standard conductance plateaus at integer values of G_0. In the model we investigated, these can be accounted for by the formation of density and spin-dependent barriers in the QPC region which can act as spin filters. Under the right circumstances, the filtering effect is strong enough that two spin-down modes can pass through the QPC before even one spin-up mode is transmitted. The barriers also acquire additional 'shoulder' structure which can create a local potential well for one spin species in the center of the QPC. In conjunction with this, we found that a local spin moment was formed in the center, though it could be best described as weakly bound for the case presented here. The appearance of such 'shoulders' in the potentials at more negative gate voltages was found to be a rather generic occurrence. However, a major effect of changing n_{1D} is to change the barrier heights and thus their relative transparency. Thus, a barrier structure that yielded a plateau in one instance could yield instead an

inflection in the conductance in another. The formation of spin-dependent barriers to electron transmission when a small number of modes is transmitted through the QPC is a result that other authors have also obtained [10, 12, 32, 36], though the specific results were different, not surprising, given that the model initial confining potentials were not the same and other choices for parameters were employed. In this regard, it should be noted that significant differences have been observed *experimentally* when QPCs of different shapes were directly compared [37].

Importantly, there is still little consensus on the physical mechanism that breaks symmetry and lifts the spin degeneracy in the channel. In numerical calculations, the spin-symmetry is *artificially* broken, in our case by introducing a weak Zeeman splitting ($\sim 10^{-6}$ eV) that is turned off after the first few iterations. Others have made use of similar approaches, but in experiment some physical mechanism should be responsible for the appearance of the spin-dependent barriers. One possibility is the exchange energy cost associated with electron occupation in the QPC channel, while another source may be a Rashba mechanism. While the Rashba effect does not normally give rise to a bulk spin polarization [38], its effect as a perturbation may be sufficient to induce the required symmetry breaking in the QPC. However, some [4] have disputed the possibility of such an effect, and this is clearly an issue requiring further careful study. We currently are in the process of doing QPC simulations that incorporate the Rashba effect.

References

[1] Wharam D A, Thornton T J, Newbury R, Pepper M, Ahmed H, Frost J E F, Hasko D G, Peacock D C, Ritchie D A and Jones G A C 1988 *J. Phys.* C **21** L209

[2] van Wees B J, van Houten H, Beenakker C W J, Williamson J G, Kouwenhoven L P, van der Marel D and Foxon C T 1988 *Phys. Rev. Lett.* **60** 848

[3] Büttiker M 1990 *Phys. Rev.* B **41** 7906

[4] Thomas K J, Nicholls J T, Simmons M Y, Pepper M, Mace D R and Ritchie D A 1996 *Phys. Rev. Lett.* **77** 135

[5] Kristensen A, Bruus H, Hansen A E, Jensen J B, Lindelof P E, Marckmann C J, Nygård J, Sørensen C B, Beuscher F, Forchel A and Michel M 2000 *Phys. Rev.* B **62** 10950

[6] Reilly D J, Facer G R, Dzurak A S, Kane B E, Stiles P J, Clark R G, Hamilton A R, Pfeiffer L N and West K W 2001 *Phys. Rev.* B **63** 121311

[7] Cronenwett S M, Lynch H J, Goldhaber-Gordon D, Kouwenhoven L P, Marcus C M, Hirose K, Wingreen N S and Umansky V 2002 *Phys. Rev. Lett.* **88** 226805

[8] Reilly D J, Buehler T M, O'Brien J L, Hamilton A R, Dzurak A S, Clark R G, Kane B E, Pfeiffer L N and West K W 2002 *Phys. Rev. Lett.* **89** 246801

[9] Meir Y, Hirose K and Wingreen N S 2002 *Phys. Rev. Lett.* **89** 196802

[10] Berggren K-F and Yakimenko I I 2002 *Phys. Rev.* B **66** 085323

[11] Hirose K, Meir Y and Wingreen N S 2003 *Phys. Rev. Lett.* **90** 026804

[12] Jaksch P, Yakimenko I and Berggren K-F 2006 *Phys. Rev.* B **74** 235320

[13] Cornaglia P S and Balseiro C A 2004 *Europhys. Lett.* **67** 634

[14] Akis R and Ferry D K 2006 *Nonequilibrium Carrier Dynamics in Semiconductors, Proc. 14th Int. Conf. (Chicago, USA, July)* (Berlin: Springer) pp 163–7

[15] Shailos A, Ashok A, Bird J P, Akis R, Ferry D K, Goodnick S M, Lilly M P, Reno J L and Simmons J A 2006 *J. Phys.: Condens. Matter* **18** 1715

[16] Gunawan O, Habib B, De Poortere E P and Shayegan M 2006 *Phys. Rev.* B **74** 155436

[17] Morimoto T, Iwase Y, Aoki N, Sasaki T, Ochiai Y, Shailos A, Bird J P, Lilly M P, Reno J L and Simmons J A 2003 *Appl. Phys. Lett.* **82** 3952

[18] Puller V I, Mourokh L G, Shailos A and Bird J P 2004 *Phys. Rev. Lett.* **92** 96802

[19] Puller V I, Mourokh L G, Bird J P and Ochiai Y 2005 *J. Phys.: Condens. Matter* **17** 5269

[20] Mourokh L, Puller V I, Smirnov A Yu and Bird J P 2005 *Appl. Phys. Lett.* **87** 192501

[21] Yoon Y, Mourokh L, Morimoto T, Aoki N, Ochiai Y, Reno J L and Bird J P 2007 *Phys. Rev. Lett.* **99** 136805

[22] Timp G 1992 *Semicond. Semimet.* **35** 113

[23] Kohn W and Sham L J 1965 *Phys. Rev.* **140** A1133

[24] Tanatar B and Ceperly D M 1989 *Phys. Rev.* B **39** 505

[25] Stern F 1973 *Phys. Rev. Lett.* **30** 278

[26] Reimann S M and Manninen M 2002 *Rev. Mod. Phys.* **74** 1283

[27] Sun Y and Kirczenow G 1993 *Phys. Rev.* B **47** 4413

[28] Wang C-K and Berggren K-F 1996 *Phys. Rev.* B **54** 14257
Wang C-K and Berggren K-F 1998 *Phys. Rev.* B **57** 4552

[29] Usuki T, Saito M, Takatsu M, Kiehl R A and Yokoyama N 1995 *Phys. Rev.* B **52** 8244

[30] Ko D Y K and Inkson J C 1988 *Phys. Rev.* B **38** 9945

[31] Akis R, Bird J P, Vasileska D, Ferry D K, deMoura A P S and Lai Y-C 2003 *Electron Transport in Quantum Dots* (Boston: Kluwer Academic) pp 209–76

[32] Starikov A A, Yakimenko I I and Berggren K-F 2003 *Phys. Rev.* B **67** 235319

[33] Shelykh I A, Bagraev N T and Klyachkin L E 2003 *Semiconductors* **37** 1390

[34] Hirose K and Wingreen N S 2001 *Phys. Rev.* B **64** 073305

[35] For a recent review, see Tarucha S, Ono K, Fujisawa T, van der Wiel W G and Kouwenhoven L P 2003 *Electron Transport in Quantum Dots* (Boston: Kluwer Academic) pp 1–42

[36] Tokura Y and Khaetskii A 2002 *Physica* E **12** 711

[37] Morimoto T, Henmi M, Naito R, Tsubaki K, Aoki N, Bird J P and Ochiai Y 2006 *Phys. Rev. Lett.* **97** 136805

[38] Winkler R 2003 *Spin-Orbit Coupling Effects in Two-Dimensional Electron and Hole Systems* (*Springer Tracts in Modern Physics* vol 191) (Berlin: Springer)